Springer

KSME

Journal of Mechanical Science and Technology 26 (4) (2012) 985~992
www.springerlink.com/content/1738-494x
DOI 10.1007/s12206-011-1006-7

Nonlinear vibration and rippling instability for embedded carbon nanotubes †

Payam Soltani[1,*], D. D. Ganji[3], I. Mehdipour[1] and A. Farshidianfar[2]

[1]*Department of Mechanical Engineering ,Semnan Branch, Islamic Azad University, Semnan, Iran*
[2]*Department of Mechanical Engineering, Ferdowsi University of Mashhad, Mashhad, Iran*
[3]*Department of Mechanical Engineering, Babol University of Technology, Babol, Iran*

(Manuscript Received November 12, 2010; Revised August 9, 2011; Accepted August 25, 2011)

Abstract

Based on the rippling deformations, a nonlinear continuum elastic model is developed to analyze the transverse vibration of single-walled carbon nanotubes (SWCNTs) embedded on a Winkler elastic foundation. The nonlinear natural frequency has been derived analytically for typical boundary conditions using the perturbation method of multi-scales. The results indicate that the nonlinear resonant frequency due to the rippling is related to the stiffness of the foundation, the boundary conditions, the excitation load-to-damping ratio, and the diameter-to-length ratio. Moreover, the rippling instability of carbon nanotubes, as a structural instability, is introduced and the influences of several effective parameters on this kind of instability are widely discussed.

Keywords: Carbon nanotube; Bending deformation; Ripple deformation; Nonlinear vibration; Winkler foundation

1. Introduction

Carbon nanotubes (CNTs) were discovered by Sumio Iijima in 1991 [1]. Because of their novel electronic, mechanical, and other physical and chemical properties, CNTs have received extensive interest, drawn a great deal of research of science and hold substantial promise as building blocks for nanotechnology [2-8]. There are several reasons confirming that accurate theoretical models for vibrational behavior of carbon nanotubes (CNTs) are very important. For instance, most of the nanodevices such as nano resonators work on the basis of vibrating CNTs. Hence, the natural frequencies of nanotubes play a significant role on the operation of nano-electromechanical systems (NEMS). In addition, the effective Young's modulus of a nanotube can be determined indirectly from its measured natural frequencies or mode shapes if a sufficiently precise theoretical model is used.

Molecular dynamics (MD) method simulates the mechanical behavior of CNTs accurately. However, MD simulation is limited to systems with a small number of atoms (say less than 10^{16}), remains time consuming and expensive [8]. For large-scale systems, continuum mechanics approach has widely and successfully modeled vibrational characteristics of CNTs and there are many researches use this method for modeling nano-structures and nanotubes recently [9-13].

The high elastic modulus of CNT (higher than 1 TPa) and remarkable bending flexibility (up to 20%) without breaking, exhibit new phenomena in bending vibration of nanotubes, called rippling deformations. This configuration affects directly the resonant frequencies, the bending stiffness, and the effective Young's modulus of a CNT. Liu et al. [14] determined the Young's modulus of a CNT by measuring resonance frequency and using the modulus-frequency relation resulting from the linear vibration theory. They showed that the Young's modulus of CNT decreased sharply, from about 1 to 0.1 TPa with increasing diameter D from 8 to 40 nanometers, corresponding to unusual rippling mode in bending. Furthermore, the investigators confirmed that the results from linear bending theory might be invalid in such measurements. Hence, a nonlinear generalized local quasi-continuum method was applied to investigate the effective stiffness of multi-walled carbon nanotubes (MWCNTs) with rippling deformation by Arroyo and Belytschko [15]. They found that the predicted effective modulus both in bending, and torsional deformations were much smaller than those predicted by linear elasticity. Wang et al. [16] constructed a three-dimensional finite element model based on orthotropic theory of finite elasticity deformation, to obtain a nonlinear bending moment–curvature relationship of CNTs, which represented the rippling deformation in bending mode. Utilizing this relationship, the effective bending modulus of carbon nanotubes with different cross-sections was obtained by means of a bi-linear theory and a simplified vibration analysis method. A more precise model was developed by Wang et al. [17] to estimate

*Corresponding author. Tel.: + 989121075452
E-mail address: payam.soltani@gmail.com; soltanip2@asme.org
† Recommended by Associate Editor Cheolung Cheong

the effective bending modulus of CNT with the rippling configuration. The bending moment–curvature relationship was derived using finite element method, expressed as a ninth order polynomial equation. A nonlinear vibration analysis method was used to calculate the effective modulus of a CNT with rippling mode. The results declared that the effective bending modulus of carbon nanotubes decreased substantially with increasing diameter.

Moreover, in recent years, many investigations have been devoted to the application of CNTs as a reinforced phase in nanocomposites and considerable attention is focused on mechanical and vibrational behaviors of CNTs embedded in an elastic matrix such as polymer and metal [7, 10].

The wavelike rippling morphology of a CNT in bending deformation affects the structural characteristics and causes the bending stiffness to be a function of deformation. Hence, in a vibrating CNT, the vibrational behavior becomes related to the dynamical deformation and instantaneous curvature of nanotube. Furthermore, the rippling deformation makes the relation between the bending stiffness and the deformation nonlinear [16, 17], and the linear bending theory is not applicable and appropriate to the transverse vibration of CNTs. The motivation behind this study is to investigate the nonlinear effects of the rippling configuration on the vibrational behavior and stability of CNTs.

In the present work, based on the rippling phenomena, a nonlinear elastic beam model is improved for transverse vibration of a single-walled carbon nanotube (SWCNT) on an elastic foundation. Following this model, the nonlinear resonant frequency is derived using the perturbation method of multi-scales for the case of typical and standard boundary conditions. The influences of the medium stiffness, boundary conditions, the excitation load-to-damping ratio, and the diameter-to-length ratio on the nonlinear resonant frequency are discussed. Additionally, for the first time, the structural instability caused by rippling deformations is introduced and the influences of the various parameters on the stability of vibrating CNTs are widely explained.

2. Vibration model

The equation of vibration of a SWCNT on an elastic foundation with a harmonic excitation force $F(x, t)$, caused by an external electrical field, can be expressed as

$$M''(x,t) + k_e w(x,t) + 2\mu \dot{w}(x,t) + \rho A \ddot{w}(x,t) = F(x,t) \quad (1a)$$

$$F(x,t) = G(x)\cos(\tilde{\omega} t) \quad (1b)$$

where $M(x, t)$ denotes the bending moment, $w(x, t)$ the beam deflection function, k_e Winkler constant determined by the material stiffness of the surrounding elastic medium, μ the damping coefficient of CNT, $F(x, t)$ the excitation load measured per unit length, and $w'(x,t)$ and $\dot{w}(x,t)$ the partial derivatives $\frac{\partial w(x,t)}{\partial x}$ and $\frac{\partial w(x,t)}{\partial t}$, respectively.

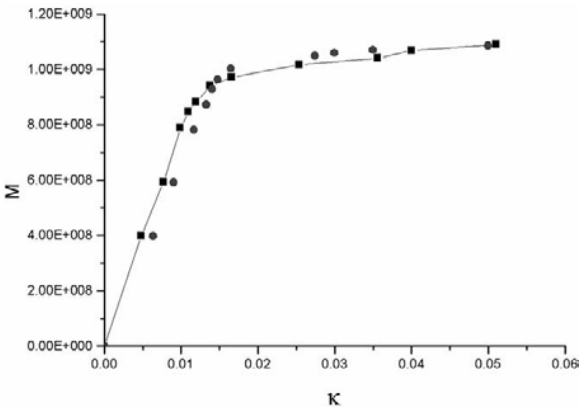

Fig. 1. The bending moment of CNT against the bending curvature for two different L/D [17].

2.1 Boundary conditions

In this research, typical boundary conditions named clamped-clamped (C-C), cantilever or clamped-free (C-F), hinged-hinged (H-H) and clamped-hinged (C-H) boundary conditions have been noticed to analyze the effects of the stiffness due to the boundaries of CNTs as follows:

C-C boundary conditions:

$$w(0,t) = w'(0,t) = 0, \quad w(L,t) = w'(L,t) = 0 \quad (2)$$

C-F boundary conditions:

$$w(0,t) = w'(0,t) = 0, \quad w''(L,t) = w'''(L,t) = 0 \quad (3)$$

H-H boundary conditions:

$$w(0,t) = w''(0,t) = 0, \quad w(L,t) = w''(L,t) = 0 \quad (4)$$

C-H boundary conditions:

$$w(0,t) = w'(0,t) = 0, \quad w(L,t) = w''(L,t) = 0. \quad (5)$$

2.2 Nonlinear vibration model

When a CNT bends, the rippling formation occurs specially for the relatively and locally large deformation. In these cases, the linear relationship between bending moment and curvature of the CNT is not applicable anymore. The nonlinear effect of rippling mode for a bent CNT has been calculated using FEM simulation [17]. Fig. 1 shows the bending moment M versus the bending curvature κ with the length-to-diameter ratios *L/D* = 10, and 20 from FEM simulating results [17].

Using beam bending theory and curve fitting technique, a ninth order polynomial equation can be introduced the behavior of bending moment M against the bending curvature κ [17].

$$M(x,t) = EI\kappa\left(1 - a_3 D^2\kappa^2 + a_5 D^4\kappa^4 - a_7 D^6\kappa^6 + a_9 D^8\kappa^8\right) \quad (6)$$

where $\kappa = \kappa(x,t)$, $a_3 = 1.755\times10^3$, $a_5 = 2.0122\times10^6$, $a_7 = 1.115\times10^9$ and $a_9 = 2.266\times10^{11}$.

The two orders of partial derivatives with respect to x in Eq. (1), gives

$$M''(x,t) = EI[\kappa''\begin{pmatrix}1-3a_3D^2\kappa^2+5a_5D^4\kappa^4-7a_7D^6\kappa^6\\+9a_9D^8\kappa^8\end{pmatrix} + (\kappa')^2\left(-6a_3D^2\kappa+20a_5D^4\kappa^3-42a_7D^6\kappa^6-72a_9D^8\kappa^7\right)]. \quad (7)$$

Based on the large deflection deformation, the relation between the bending curvature $\kappa(x,t)$ and the beam deflection $w(x,t)$ can be expressed as

$$\begin{aligned}\kappa(x,t) &= \frac{w''(x,t)}{\left[1+w'(x,t)^2\right]^{3/2}} \\ &= w''\left[1-\frac{3}{2}(w')^2+\frac{15}{8}(w')^4-\cdots\right] \\ &\cong w''(x,t)\left[1-r(w')^2\right]\end{aligned} \quad (8)$$

where substituting Eq. (8) into Eq. (7), yields

$$\begin{aligned}M''(x,t) &= EI\{w'''' - 3a_3D^2\left[2w''(w''')^2+(w'')^2w''''\right] \\ &-r\left[2(w'')^3+6w'w''w'''+(w')^2w''''\right]\}.\end{aligned} \quad (9)$$

The nonlinear vibration equation will be obtained by substituting Eq. (9) into Eq. (1)

$$EIw'''' + k_e w + 2\mu\dot{w} + \rho A\ddot{w} = EIN(w) + F(x,t) \quad (10a)$$

where N (w) denotes for the nonlinear part of equation as follows:

$$\begin{aligned}N(w) &= 3a_3D^2\left[2w''(w''')^2+(w'')^2w''''\right]+ \\ &r\left[2(w'')^3+6w'w''w'''+(w')^2w''''\right].\end{aligned} \quad (10b)$$

Making all the variables in Eq. (10) dimensionless by using the characteristic length L, time $L^2\sqrt{\rho A/EI}$ and force EI/L^3, gives

$$\bar{w}'''' + \bar{k}_e\bar{w} + 2\bar{\mu}\dot{\bar{w}} + \ddot{\bar{w}} = \bar{N} + \bar{F}(x^*,t^*) \quad (11a)$$

$$\bar{F}(x^*,t^*) = \bar{G}(x^*)\cos(\tilde{\omega}^*t^*) \quad (11b)$$

where

$$x^* = x/L,\ \ t^* = t\sqrt{EI/\rho A}/L^2,\ \ \bar{w} = w/L,\ \ \bar{k}_e = k_eL^4/EI,$$
$$\bar{\mu} = \mu L^2/\sqrt{EI\rho A},\ \ \bar{N} = N/L^3,\ \ \bar{G} = GL^3/EI. \quad (12)$$

The associated dimensionless boundary conditions handled in this paper are given as follows:

<u>C-C boundary conditions</u>:

$$\bar{w}(0,t^*) = \bar{w}'(0,t^*) = 0,\quad \bar{w}(1,t^*) = \bar{w}'(1,t^*) = 0 \quad (13)$$

<u>C-F boundary conditions</u>:

$$\bar{w}(0,t^*) = \bar{w}'(0,t^*) = 0,\quad \bar{w}''(1,t^*) = \bar{w}'''(1,t^*) = 0 \quad (14)$$

<u>H-H boundary conditions</u>:

$$\bar{w}(0,t^*) = \bar{w}''(0,t^*) = 0,\quad \bar{w}(1,t^*) = \bar{w}''(1,t^*) = 0 \quad (15)$$

<u>C-H boundary conditions</u>:

$$\bar{w}(0,t^*) = \bar{w}'(0,t^*) = 0,\quad \bar{w}(1,t^*) = \bar{w}''(1,t^*) = 0. \quad (16)$$

2.3 Nonlinear analysis

The fundamental linear frequency of a vibrating CNT corresponding to each previous boundary condition is introduced as ω^*. Pursuant to non-linearity, the non-linear frequency $\tilde{\omega}^*$ deviates slightly from ω^*. The perturbation method of multi-scales has been applied to calculate the resonance frequency $\tilde{\omega}$ for a CNT on elastic foundation with rippling deformation [18]. The beam deflection w can be expanded, using small perturbation parameter ε, into $u=u_0+\varepsilon u$ where the initial displacement u_0 should be zero. To make all terms in Eq. (10) be of the same order in w, the parameters $\bar{\mu} = \varepsilon^2\upsilon$ and $\bar{G}(x^*) = \varepsilon^3 g(x^*)$ are determined [17] and the non-linear Eq. (10) becomes:

$$u'''' + \bar{k}_e u + 2\varepsilon^2\upsilon\dot{u} + \ddot{u} = \varepsilon^2 N_u + \varepsilon^2 g\cos(\tilde{\omega}^*t^*) \quad (17)$$

where

$$\begin{aligned}N_u &= 3a_3(D/L)^2\left[2u''(u''')^2+(u'')^2u''''\right] \\ &+r\left[2(u'')^3+6u'u''u'''+(u')^2u''''\right].\end{aligned} \quad (18)$$

In the above formula, $u(x^*,t^*)$ and $g(x^*)$ are, respectively, expanded as

$$u(x^*,t^*) = \sum_{n=1}^{\infty} q_n(t^*)\phi_n(x^*),\quad g(x^*) = \sum_{n=1}^{\infty} g_n\phi_n(x^*) \quad (19)$$

where ϕ_n for n = 1, 2, 3 . . . represent the normalized mode functions of the beam from the linear vibration analysis due to the specified boundary condition. Meanwhile the mode function ϕ_n satisfies the following formula:

$$\int_0^1 \varphi_i(x^*)\varphi_j(x^*)dx^* = \delta_{ij} \quad i,j = 1,2,\ldots \quad (20)$$

and δ_{ij} represents Kronocker delta. Substituting Eq. (19) into Eq. (18) and utilizing Eq. (20), we have

$$\ddot{q}_1 + 2\varepsilon_1\upsilon\dot{q}_1 + (\omega_1^{*2} + \bar{k}_e)q_1 = \varepsilon_1\alpha q_1^3 + \varepsilon_1 g_1\cos(\tilde{\omega}^*t^*). \quad (21)$$

Table 1. The first order of inherence frequency due to boundary conditions.

Boundary condition	ω_1^*
C-F	3.516
C-C	22.37328786
C-H	15.41820327
H-H	9.8696044

In addition, based on linear analysis of the beams, the first order of inherence frequency corresponding to the fundamental mode of vibration ω_1^*, have been given in Table 1. According to Eq. (21), it is obvious that the fundamental linear frequency of CNT is $\omega^{*2} = \omega_1^{*2} + \bar{k}_e$.

Eq. (21) represents a third order nonlinear oscillation equation (called damping forced Duffing's equation) [18], which is yielded by the parameter α. α is the parameter depends on normalized mode functions of the beam, the associated boundary condition and the diameter-to-length of CNT. This parameter is calculated for each case as follows:

For C-C condition

$$\beta_1 = \int_0^1 \phi_1 \left[2\phi_1''(\phi_1''')^2 + (\phi_1'')^2 \phi_1''' \right] dx^* = 1.546729013 \times 10^5 \quad (22a)$$

$$\beta_2 = \int_0^1 \phi_1 \left[2(\phi_1'')^2 + 6\phi_1'\phi_1''\phi_1''' + (\phi_1')^2 \phi_1''' \right] dx^* = 2846.499985 \quad (22b)$$

$$\begin{aligned} \alpha &= 3a_3 (D/L)^2 \beta_1 + r\beta_2 \\ &\approx 3a_3 (D/L)^2 \times 1.546729013 \times 10^5 + r \times 2846.499985 \\ &\approx (28536.86783 D/L)^2 + 4269.749978 \end{aligned} \quad (23)$$

For C-F condition

$$\beta_1 = \int_0^1 \phi_1 \left[2\phi_1''(\phi_1''')^2 + (\phi_1'')^2 \phi_1''' \right] dx^* = 119.6 \quad (24a)$$

$$\beta_2 = \int_0^1 \phi_1 \left[2(\phi_1'')^2 + 6\phi_1'\phi_1''\phi_1''' + (\phi_1')^2 \phi_1''' \right] dx^* = 20.1939 \quad (24b)$$

$$\begin{aligned} \alpha &= 3a_3 (D/L)^2 \beta_1 + r\beta_2 \\ &\approx 3a_3 (D/L)^2 \times 119.6 + r \times 20.1939 \\ &\approx (793.533 D/L)^2 + 30.3555 \end{aligned} \quad (25)$$

For H-H condition

$$\beta_1 = \int_0^1 \phi_1 \left[2\phi_1''(\phi_1''')^2 + (\phi_1'')^2 \phi_1''' \right] dx^* = \frac{1}{2}\pi^8 \quad (26a)$$

$$\beta_2 = \int_0^1 \phi_1 \left[2(\phi_1'')^2 + 6\phi_1'\phi_1''\phi_1''' + (\phi_1')^2 \phi_1''' \right] dx^* = \frac{1}{2}\pi^6 \quad (26b)$$

$$\begin{aligned} \alpha &= 3a_3 (D/L)^2 \beta_1 + r\beta_2 \\ &\approx 3a_3 (D/L)^2 \times \frac{1}{2}\pi^8 + r \times \frac{1}{2}\pi^6 \\ &\approx (51.30789413\pi^4 D/L)^2 + 0.75\pi^6 \end{aligned} \quad (27)$$

For C-H condition

$$\beta_1 = \int_0^1 \phi_1 \left[2\phi_1''(\phi_1''')^2 + (\phi_1'')^2 \phi_1''' \right] dx^* = 31818.0102\ 8 \quad (28a)$$

$$\beta_2 = \int_0^1 \phi_1 \left[2(\phi_1'')^2 + 6\phi_1'\phi_1''\phi_1''' + (\phi_1')^2 \phi_1''' \right] dx^* = 1321.67787\ 9 \quad (28b)$$

$$\begin{aligned} \alpha &= 3a_3 (D/L)^2 \beta_1 + r\beta_2 \\ &\approx 3a_3 (D/L)^2 \times 31818.0102\ 8 + r \times 1321.67787\ 9 \\ &\approx (12943.0222\ 2 D/L)^2 + 1982.51681\ 8 \end{aligned} \quad (29)$$

Furthermore, the nonlinear frequency $\tilde{\omega}^*$ can be expressed by perturbation parameter ε_1 as

$$\tilde{\omega}^* = \sqrt{\omega_1^{*2} + \bar{k}_e} - \sigma\varepsilon_1. \quad (30)$$

The solution for the Eq. (21) and the dimensionless excitation force can be stated respectively as

$$q_1(t^*, \varepsilon) = q_{10}(T_0, T_1) + \varepsilon_1 q_{11}(T_0, T_1) + \cdots \quad (31a)$$

$$\varepsilon^2 g_1 \cos(\tilde{\omega}^* t^*) = \varepsilon_1^2 g_1 \cos(\sqrt{\omega_1^{*2} + \bar{k}_e} T_0 - \sigma T_1). \quad (31b)$$

Substituting Eqs. (31) into Eq. (21), and comparing coefficients of the identical power of ε_1, we have

$$(\varepsilon_1^0): D_0^2 q_{10} + \left((\omega_1^*)^2 + \bar{k}_e \right) q_{10} = 0 \quad (32a)$$

$$\begin{aligned} (\varepsilon_1^1): D_0^2 q_{11} + \left((\omega_1^*)^2 + \bar{k}_e \right) q_{11} &= -2D_0 D_1 q_{10} - 2\upsilon D_0 q_{10} \\ &+ \alpha q_{10}^3 + g_1 \cos(\omega_1^* T_0 - \sigma T_1) \end{aligned} \quad (32b)$$

where $D_n = \dfrac{\partial}{\partial T_n} (n = 0,1).$

The generating solution can be obtained from Eq. (32a)

$$q_{10} = A(T_1) e^{i\sqrt{\omega_1^{*2} + \bar{k}_e} T_0} + \bar{A}(T_1) e^{-i\sqrt{\omega_1^{*2} + \bar{k}_e} T_0}. \quad (33)$$

Substituting for q_{10} into Eq. (32b) gives

$$\begin{aligned} &D_0^2 q_{11} + \left((\omega_1^*)^2 + \bar{k}_e \right) q_{11} = \\ &\left(-2\left(\left(\frac{d}{dT_1} A(T_1) \right) + \upsilon A(T_1) \right) i\sqrt{\omega_1^{*2} + \bar{k}_e} + 3\alpha A(T_1)^2 \bar{A}(T_1) \right) e^{i\sqrt{\omega_1^{*2} + \bar{k}_e} T_0} \\ &+ \alpha A(T_1)^3 e^{3i\sqrt{\omega_1^{*2} + \bar{k}_e} T_0} + \frac{1}{2} g_1 e^{i\left(\sqrt{\omega_1^{*2} + \bar{k}_e} T_0 - \sigma T_1 \right)} + cc \end{aligned} \quad (34)$$

where *cc* stands for the complex conjugate of preceding terms.

Secular terms will be eliminated from the particular solution of Eq. (34) if we choose A to be a solution of

$$2\left(\left(\frac{d}{dT_1}A(T_1)\right)+\upsilon A(T_1)\right)i\sqrt{\omega_1^{*2}+\bar{k}_e}-3\alpha A(T_1)^2\bar{A}(T_1)-\frac{1}{2}\frac{g_1}{e^{i\sigma T_1}}=0. \tag{35}$$

To solve Eq. (35), we write A in the polar form

$$A(T_1)=\frac{1}{2}a(T_1)\exp(i\beta(T_1)) \tag{36}$$

where a and β are real functions of slow time scale T_1. Then by separating, the result into its real and imaginary parts

$$\begin{aligned} a' &= -\upsilon a-\frac{1}{2}\frac{g_1}{\sqrt{\omega_1^{*2}+\bar{k}_e}}\sin\left(\gamma(T_1)\right),\\ a\beta' &= -\frac{3}{8}\frac{\alpha}{\sqrt{\omega_1^{*2}+\bar{k}_e}}a^3+\frac{1}{2}\frac{g_1}{\sqrt{\omega_1^{*2}+\bar{k}_e}}\cos\left(\gamma(T_1)\right). \end{aligned} \tag{37}$$

where $\gamma(T_1)=\beta(T_1)+\sigma.T_1$.

For the steady-state response in the neighborhoods of singular points, every small perturbation motion has to decay, and this occurs when $\alpha'=\gamma'=0$, therefore

$$\begin{aligned} \upsilon a &= \frac{1}{2}\frac{g_1}{\sqrt{\omega_1^{*2}+\bar{k}_e}}\sin\left(\gamma\right),\\ \frac{3}{8}\frac{\alpha}{\sqrt{\omega_1^{*2}+\bar{k}_e}}a^3-a\sigma &= \frac{1}{2}\frac{g_1}{\sqrt{\omega_1^{*2}+\bar{k}_e}}\cos\left(\gamma\right). \end{aligned} \tag{38}$$

By omitting γ from Eq. (38), it can be written as

$$\upsilon^2\left(\omega_1^{*2}+\bar{k}_e\right)a^2+\left(\sigma\sqrt{\omega_1^{*2}+\bar{k}_e}-\frac{3}{8}\alpha a^2\right)a^2=\frac{1}{4}g_1^2. \tag{39}$$

In the previous equation, the maximum vibration amplitude α and phase angle β will be calculated simply by removing secular terms as

$$a=\frac{g_1}{2\sqrt{\omega_1^{*2}+\bar{k}_e}\upsilon} \tag{40}$$

and

$$\sigma\sqrt{\omega_1^{*2}+\bar{k}_e}=\frac{3}{8}\alpha a^2. \tag{41}$$

In Eq. (41), σ represents a variable of maximum vibration amplitude a and dimensionless parameter of Winkler constant $\bar{k}_e$, and is written as

$$\begin{aligned} \sigma &= \frac{3\alpha}{8\sqrt{\omega_1^{*2}+\bar{k}_e}}a^2=\frac{3\alpha}{8\sqrt{\omega_1^{*2}+\bar{k}_e}}\left(\frac{g_1}{2\sqrt{\omega_1^{*2}+\bar{k}_e}\upsilon}\right)^2\\ &= \frac{3\alpha g_1^2}{32\left(\omega_1^{*2}+\bar{k}_e\right)^{3/2}\upsilon^2}. \end{aligned} \tag{42}$$

At last, the nonlinear resonance frequency of the CNT on Winkler-like foundation with rippling effect $\tilde{\omega}^*$ can be determined as

$$\tilde{\omega}^*=\sqrt{\omega_1^{*2}+\bar{k}_e}-\sigma\varepsilon_1=\sqrt{\omega_1^{*2}+\bar{k}_e}-\frac{3\alpha g_1^2}{32\left(\omega_1^{*2}+\bar{k}_e\right)^{3/2}\upsilon^2}\varepsilon_1 \tag{43}$$

where

$$g_1=\frac{\bar{G}_1}{\varepsilon^3},\quad and\quad \upsilon=\frac{\bar{\mu}}{\varepsilon^2}. \tag{44}$$

Substituting Eq. (44) into Eq. (43).

$$\tilde{\omega}^*=\sqrt{\omega_1^{*2}+\bar{k}_e}-\frac{3\alpha\bar{G}_1^2}{32\left(\omega_1^{*2}+\bar{k}_e\right)^{3/2}\bar{\mu}^2}. \tag{45}$$

In addition, the nonlinear resonant frequency ratio r can be introduced as

$$r=\frac{\tilde{\omega}^*}{\omega^*}=1-\frac{3\alpha\bar{G}_1^2}{32\left(\omega_1^{*2}+\bar{k}_e\right)^2\bar{\mu}^2}. \tag{46}$$

3. Results and discussion

Eq. (46) represents the ratio of the nonlinear resonant frequency, caused by rippling configuration of a SWCNT, to the linear frequency. In fact, the second term of this equation reveals the nonlinearity of the model, caused by the rippling formation. As it is seen, this nonlinearity is a function of linear natural frequency ω_1^*, Winkler constant $\bar{k}_e$, exciting load-to-damping ratio , boundary conditions, and diameter-to-length ratio $\frac{D}{L}$. According to this model and for verification, the obtained nonlinear frequency has been adopted with results from Refs. [13] and [16] which shows good agreement in the case of long slender CNTs without the elastic medium.

In Fig. 2, the nonlinear frequency ratio r is plotted as a function of dimensionless Winkler constant $\bar{k}_e$ for different values of D/L with C-C boundary condition. As it shows, while the excitation load-to-damping ratio $\bar{G}_1/\bar{\mu}$ remains constant, the nonlinear frequency decreases with increasing the diameter-to-length ratio D/L. Moreover, for a given value of D/L, as the stiffness of medium increases, the nonlinear effects of

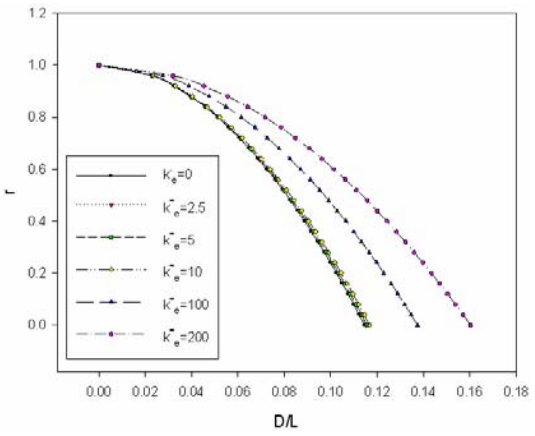

Fig. 2. The effects of Winkler constant $\bar{k}_e$ on the nonlinear frequency ratio with C-C condition when $\overline{G_1}/\mu = 0.5$.

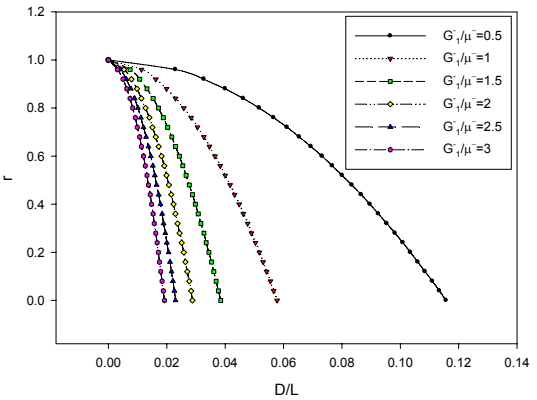

Fig. 3. The effects of excitation load-to-damping ratio on the nonlinear frequency ratio with C-C condition when $\bar{k}_e$=5.

rippling formation decreases and the nonlinear frequency ratio *r* tends to 1. Meanwhile, for the long slender CNTs with D/L smaller than 0.02, the nonlinear frequency ratio is approximately equal one ($r \cong 1$) for all values of dimensionless Winkler constants $\bar{k}_e$. In this case, the nonlinear effects of rippling deformation can be neglected and the geometric nonlinearity of the structure can be out of account.

The effect of the excitation load-to-damping ratio on the nonlinear frequency has been plotted in Fig. 3 for $\bar{K}_e = 5$. It can be seen from the figure that the nonlinear frequency ratio *r* decreases sharply for large values of D/L, especially when the excitation load-to-damping ratio $\overline{G_1}/\mu$ is almost high. In other words, the nonlinear effect of rippling deformation exaggerates by raising the excitation load amplitude or by reduction of the damping of the model.

Another important factor, which influences on the nonlinear resonant frequency of CNT, is boundary conditions. α is the parameter which represents this effect in Eq. (26) and causes changing in the nonlinear frequency ratio *r* . Figs. 4-6 show the variation of *r* with D/L for the typical boundary conditions

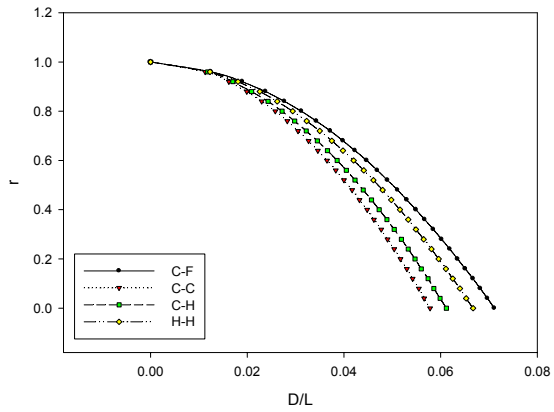

Fig. 4. The effects of boundary conditions on the nonlinear frequency ratio when. $\bar{k}_e = 5, \frac{\overline{G_1}}{\mu} = 1$.

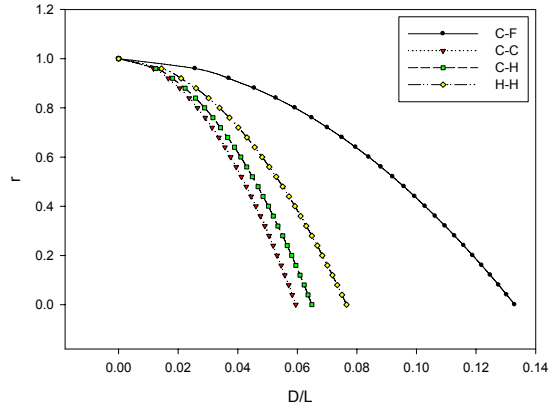

Fig. 5. The effects of boundary conditions on the nonlinear frequency ratio when $\bar{k}_e = 20, \frac{\overline{G_1}}{\mu} = 1$.

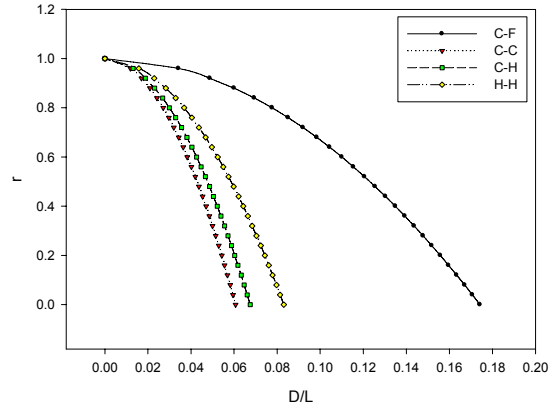

Fig. 6. The effects of boundary conditions on the nonlinear frequency ratio when $\bar{k}_e = 30, \frac{\overline{G_1}}{\mu} = 1$.

mentioned in the previous section. In all of these figures, the excitation load-to-damping ratio $\frac{\overline{G_1}}{\mu}$ is equal to 1 while the

dimensionless Winkler constant $\bar{k}_e$ is 5, 20 and 30 respectively. According to these figures, for a CNT with a given diameter to length ratio D/L, by reducing the stiffness of the system, due to the boundary conditions, the effect of rippling nonlinearity decreases and the ratio *r* take values closer to 1. Furthermore, for CNTs with small values of D/L (say $D/L < 0.02$), the nonlinear frequency ratio *r* is very close to 1 especially when the stiffness of the medium is relatively small (see Fig. 4). Hence, for long slender CNTs embedded in a soft elastic medium, the effect of rippling deformation can be ignored.

Rippling formation may cause structural instability on the vibrating CNT under certain conditions, especially in locally large deformations. Indeed, in this case, the presence of wave-like configurations of the inner side of the bent CNT should diminish bending stiffness to zero, and lead to the vibrational amplitude approaches infinity. In our model, when the nonlinear frequency ratio *r* takes non-positive values, the model shows rippling instability. Hence, the instability threshold is introduced as *r=0*. Consequently, the effects of variables influence on the rippling instability can be calculated from Eq. (46). In the instability threshold (*r* = 0), the variations of diameter-to-length *D/L* against Winkler constant and boundary conditions are shown in Figs. 7-9 while the load-to-damping ratio $\bar{G}_1/\bar{\mu}$ remains constant in each figure. It is seen that rippling instability happens in larger values of D/L as the surrounding stiffness rises. In other words, as the foundation of vibrating CNT becomes stiffer, the instability due to rippling occurs in CNTs with the larger diameter in the constant length.

Our investigation shows that boundary condition is another important factor, which influences on the rippling instability. As the stiffness of the model due to the boundary conditions decreases form C-C to C-F, (in Figs. 7-9) rippling instability occurs in larger values of D/L in the same Winkler constant. Meanwhile, when the stiffness of medium is relatively small, the different between curves decreases and rippling instability happens almost in the same D/L for all kinds of boundary conditions. This means that for very compliant and soft mediums, instability should occur in the same values of D/L regardless of the end conditions of CNTs. In addition, as it is seen in these figures, the slopes of C-C curves are near to zero, and in consequence, the effect of Winkler constant can be ignored while, for C-F, the stiffness of the surrounding medium plays an important role on the rippling instability.

4. Conclusion

Based on the rippling deformation, a nonlinear elastic beam model was presented for transverse vibration of a SWCNT. The stiffness of medium was included in the formulation as Winkler foundation to determine the vibration behavior of CNT more precisely for embedded CNTs. The nonlinear frequency ratio has been derived for C-C, C-H, H-H and C-F boundary conditions. Results predicted by present model show that the stiffness of medium (Winkler constant), boundary

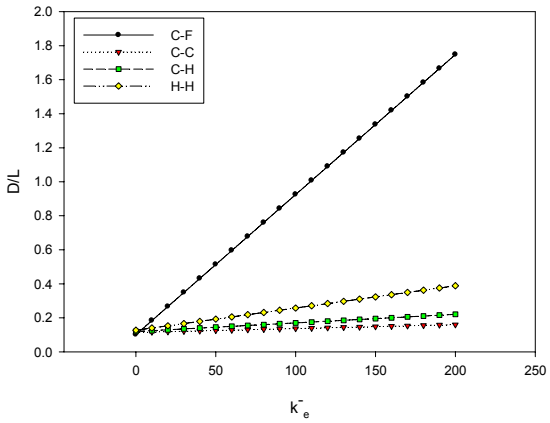

Fig. 7. The effects of Winkler constant $\bar{k}_e$ and boundary conditions on the stability of CNT due to rippling when $\frac{\bar{G}_1}{\bar{\mu}}=0.5$.

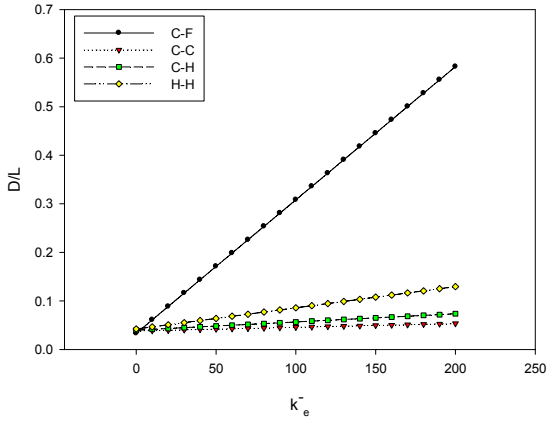

Fig. 8. The effects of Winkler constant $\bar{k}_e$ and boundary conditions on the stability of CNT due to rippling when $\frac{\bar{G}_1}{\bar{\mu}}=1.5$.

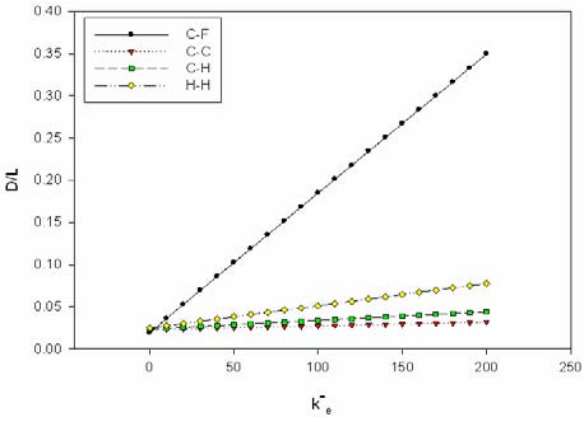

Fig. 9. The effects of Winkler constant $\bar{k}_e$ and boundary conditions on the stability of CNT due to rippling when $\frac{\bar{G}_1}{\bar{\mu}}=2.5$.

conditions, the diameter-to-length ratio and the excitation load-to-damping ratio affect the nonlinear frequency obviously. As the Winkler constant decreases or the excitation load-to-damping ratio increases the nonlinearity effect due to rippling increases.

Moreover, for the first time, the rippling instability has been introduced as a structural instability. In fact, the appearance of wavelike distortion on the inner radius of the bent CNT diminishes the bending stiffness and may lead to nanotube becomes unstable. Our nonlinear analysis can predict the conditions deal with the rippling instability and indicates that as the stiffness of the medium and/or the stiffness due to the boundary condition decrease, the rippling instability happens in smaller values of the diameter-to-length ratio.

References

[1] S. Iijima, Helical microtubules of graphitic carbon, *Nature*, 354 (1991) 56-58.

[2] A. Bachtold, P. Hadley, T. Nakanishi and C. Dekker, Logic circuits with carbon nanotube transistors, *Science*, 294 (2001) 1317.

[3] E. W. Wong, P. E. Sheehan and C. M. Lieber, Nanobeam mechanics: elasticity, strength, and toughness of nanorods and nanotubes, *Science*, 277 (1997) 1971.

[4] K. Tsukagoshi, N. Yoneya, S. Uryu, Y. Aoyagi, A. Kanda, Y. Ootuka and B. Alphenaar, Carbon nanotube devices for nanoelectronics, *Physica B: Condensed Matter*, 323 (2002) 107-114.

[5] B. Hornbostel, P. Pötschke, J. Kotz and S. Roth, Mechanical properties of triple composites of polycarbonate, single-walled carbon nanotubes and carbon fibres, *Physica E: Low-dimensional Systems and Nanostructures*, 40 (2008) 2434-2439.

[6] R. H. Baughman, A. A. Zakhidov and W. A. De Heer, Carbon nanotubes the route toward applications, *Science,* 297 (2002) 787.

[7] E. T. Thostenson, Z. Ren and T. W. Chou, Advances in the science and technology of carbon nanotubes and their composites: a review, *Composites Science and Technology*, 61 (2001) 1899-1912.

[8] R. F. Gibson, E. O. Ayorinde and Y. F. Wen, Vibrations of carbon nanotubes and their composites: a review, *Composites Science and Technology*, 67 (2007) 1-28.

[9] M. A. Hawwa and H. M. Al-Qahtani, Nonlinear oscillations of a double-walled carbon nanotube, *Computational Materials Science*, 48 (2010) 140-143.

[10] T. Murmu and S. Pradhan, Thermo-mechanical vibration of a single-walled carbon nanotube embedded in an elastic medium based on nonlocal elasticity theory, *Computational Materials Science*, 46 (2009) 854-859.

[11] Y. Zhang, G. Liu and X. Han, Transverse vibrations of double-walled carbon nanotubes under compressive axial load, *Physics Letters A*, 340 (2005) 258-266.

[12] S. Gupta and R. Batra, Continuum structures equivalent in normal mode vibrations to single-walled carbon nanotubes, *Computational Materials Science*, 43 (2008) 715-723.

[13] Y. Fu, J. Hong and X. Wang, Analysis of nonlinear vibration for embedded carbon nanotubes, *Journal of Sound and Vibration,* 296 (2006) 746-756.

[14] J. Z. Liu, Q. Zheng and Q. Jiang, Effect of a rippling mode on resonances of carbon nanotubes, *Physical Review Letters*, 86 (2001) 4843-4846.

[15] M. Arroyo and T. Belytschko, Nonlinear mechanical response and rippling of thick multiwalled carbon nanotubes, *Physical Review Letters*, 91 (2003) 215505.

[16] X. Wang, Y. Zhang, X. Xia and C. Huang, Effective bending modulus of carbon nanotubes with rippling deformation, *International Journal of Solids and Structures*, 41 (2004) 6429-6439.

[17] X. Wang, X. Wang and J. Xiao, A non-linear analysis of the bending modulus of carbon nanotubes with rippling deformations, *Composite Structures*, 69 (2005) 315-321.

[18] A. H. Nayfeh and D. T. Mook, Nonlinear oscillations, *Wiley Online Library*, 1979.